**AALBORG
UNIVERSITY**

Prediction of ground reaction forces and moments during sports-related movements

Skals, Sebastian Laigaard; Jung, Moonki; Damsgaard, Michael; Andersen, Michael Skipper

Prediction of ground reaction forces and moments during sports-related movements

Sebastian Skals[1,2], Moon Ki Jung[3], Michael Damsgaard[3], Michael S. Andersen[4]

[1]*National Research Centre for the Working Environment, Lersø Parkallé 105, DK-2100 Copenhagen East, Denmark*

[2]*Department of Health Science and Technology, Aalborg University, Fredrik Bajers Vej 7D, DK-9220 Aalborg East, Denmark*

[3]*AnyBody Technology A/S, Niels Jernes Vej 10, DK-9220 Aalborg East, Denmark*

[4]*Department of Mechanical and Manufacturing Engineering, Aalborg University, Fibigerstraede 16, DK-9220 Aalborg East, Denmark*

Corresponding author:

Michael Skipper Andersen, M.Sc.E.E., Ph.D.

Phone: +45-99409311

Mobile: +45-30354170

E-mail: msa@m-tech.aau.dk

Abstract

When performing inverse dynamic analysis (IDA) of musculoskeletal models to study human motion, inaccuracies in experimental input data and a mismatch between model and subject lead to dynamic inconsistency. By predicting the ground reaction forces and moments (GRF&Ms), this inconsistency can be reduced and force plate measurements become unnecessary. In this study, a method for predicting GRF&Ms was validated for an array of sports-related movements. The method was applied to ten healthy subjects performing e.g. running, a side-cut manoeuvre, and vertical jump. Pearson's correlation coefficient (r) and root-mean-square deviation were used to compare the predicted GRF&Ms and associated joint kinetics to a traditional IDA approach, where the GRF&Ms were measured using force plates. The main findings were that the method provided estimates comparable to traditional IDA across all movements for vertical GRFs (r ranging from 0.97 to 0.99, median 0.99), joint flexion moments (r ranging from 0.79 to 0.98, median 0.93), and resultant joint reaction forces (r ranging from 0.78 to 0.99, median 0.97). Considering these results, this method could be used instead of force plate measurements, hereby, facilitating IDA in sports science research and enabling complete IDA using motion analysis systems that do not incorporate force plate data.

Keywords: Musculoskeletal model; inverse dynamics; sports science; AnyBody Modeling System; force plates.

Abbreviations:

Inverse dynamic analysis (IDA)

Ground reaction forces and moments (GRF&Ms)

Acceleration from a standing position (ASP)

AnyBody Modeling System (AMS)

Degrees-of-freedom (DOF)

Ground reaction force (GRF)

Ground reaction moment (GRM)

Ankle flexion moment (AFM)

Ankle subtalar eversion moment (ASEM)

Knee flexion moment (KFM)

Hip flexion moment (HFM)

Hip abduction moment (HAM)

Hip external rotation moment (HERM)

Joint reaction force (JRF)

Pearson's correlation coefficient (r)

Root-mean-square deviation (RMSD)

Right leg (RL)

Left leg (LL)

1. Introduction

Musculoskeletal modelling is an important tool for understanding the internal mechanisms of the body during motion. To this day, it remains very challenging to measure muscle, ligament, and joint forces in vivo, and the associated procedures are invasive. Therefore, the use of musculoskeletal models for estimating these forces have become widespread and contribute important information to a variety of scientific fields, such as clinical gait analysis [1], ergonomics [2], orthopaedics [3], and sports biomechanics [4].

There exist a number of different analytical approaches within musculoskeletal modelling, as for instance forward dynamics-based tracking methods [5], EMG-driven forward dynamics [6], dynamic optimization [7], and inverse dynamic analysis (IDA) [8]. In IDA, measurements of body motion and external forces are input to the equations of motion, and the joint reaction and muscle forces can be computed in a process known as muscle recruitment [8, 9]. Typically, marker-based motion analysis and force plate measurements are used to determine body segment kinematics (i.e., positions, velocities, and accelerations) [10] and ground reaction forces and moments (GRF&Ms) [11], respectively, while the body segment parameters (i.e., segment mass, centre-of-mass, and moment-of-inertia) are determined through cadaver-based studies [12] and model scaling techniques [13].

It is well-known that the results of IDA are sensitive to inaccuracies in these input data [14, 15]. In addition, when analysing full-body models, the system becomes over-determinate as the GRF&Ms are input to the equations of motion [16-18]. In some cases, it can be justifiable to solve this over-determinacy by simply discarding acceleration measurements for one or more segments in the

model. When this is not possible, however, the dynamic inconsistency arising from these two issues can be solved by introducing residual forces and moments in the model to obtain dynamic equilibrium [17-19].

In order to improve dynamic consistency, these residual forces and moments have been used to reduce error effects from the input data through various optimization methods [17, 18, 20]. Alternatively, dynamic consistency can be improved by deriving the GRF&Ms from the model kinematics and segment dynamical properties only, which is commonly known as the top-down approach [17, 20]. This method has traditionally been limited by the fact that the inverse dynamics problem becomes indeterminate during double-contact phases, where the system forms a closed kinetic chain [19, 21]. In recent years, however, several studies have provided solutions to this issue [19, 21-25]. For example, Fluit et al. [19] demonstrated a universal method for predicting GRF&Ms using kinematic data and a scaled musculoskeletal model only, in which the indeterminacy issue was solved by computing the GRF&Ms as part of the muscle recruitment algorithm. Additionally, compliant foot-ground contact models have also been developed, where the ground reaction forces (GRFs) are estimated based solely on the relative position and velocity between the segments of the foot and a ground plane [26]. This is accomplished by introducing springs, dampers, and friction between the foot and ground. While this approach comes close to the physical interaction between bodies in contact, it does not model the inherent ability of the human body to shift the load from one leg to the other during double support.

Besides improving dynamic consistency, predicting the GRF&Ms obviates the need for force plate measurements, which has some additional advantages: 1) the measurement errors associated with force plates can be eliminated, 2) force plate targeting can be avoided – an issue that may affect the segment angles and

5

GRF&Ms [27], and 3) it facilitates IDA of movements that are continuous and occupy a large space [22]. Furthermore, while motion analysis systems that are able to operate outdoors are currently available, force plates are difficult and expensive to install in multi-settings [22], and are sensitive to temperature and humidity variations [11]. For sports science research, predicting GRF&Ms would be particularly advantageous. Ensuring force plate impact during sports-related movements that are highly dynamic and require large amounts of space can be difficult. This issue could restrict natural execution of the movement or even require force plate targeting to ensure impact, hereby, potentially compromising the quality of the measurements. Finally, several sports-related movements can only be analysed in their entirety in an outdoor environment, which is currently infeasible using force plates. However, none of the existing methods for predicting GRF&Ms have been validated for sports-related movements.

Therefore, the aim of this study was to evaluate the accuracy of the method proposed by Fluit et al. [19] to predict GRF&Ms during sports-related movements. This was accomplished by performing IDA on a variety of movements, such as running, vertical jump, and a side-cut manoeuvre. For validation, the predicted GRF&Ms and associated joint kinetics were compared to the corresponding variables obtained from a model, in which the GRF&Ms were measured using force plates. If comparable accuracy between these two methods can be established, it would provide new and valuable opportunities for IDA in sports science research.

2. Materials and methods

2.1 Experimental procedures

Ten healthy subjects (8 males and 2 females, age: 25.70 ± 1.49 years, height: 180.80 ± 7.39 cm, weight: 76.88 ± 10.37 kg) volunteered for the study and provided written informed consent. During measurements, male subjects only wore tight fitting underwear or running tights, while female subjects also wore a sports-brassiere. In addition, all subjects wore a pair of running shoes in their preferred size, specifically the *Brooks Ravenna 2* (Brooks Sports Inc., Seattle, WA, US), in order to minimize discomfort and, hereby, facilitate natural execution of the movements.

A 5 min warm-up at 160 W was completed on a cycle ergometer before multiple practice trials were performed. The practice trials served two overall purposes and were preceded by a thorough instruction: for each movement, multiple repetitions were performed to ensure consistent technique throughout the duration of the experiment and establish a starting position from which the subjects were able to consistently impact the force plates. When the subjects were able to perform three consecutive repetitions with adequate technique, while consistently impacting the force plates, their starting position was marked and they were given a brief pause before markers were taped to their skin.

The following movements were included in the study: 1) running, 2) backwards running, 3) a side-cut manoeuvre, 4) vertical jump, and 5) acceleration from a standing position (ASP). These movements were chosen because they represent some of the most common movements associated with sports and recreational exercise, and can be performed without specialised skills. The movements also provided varied characteristics in the resulting GRF&Ms,

considering factors such as force plate impact time, force magnitude and direction, while involving both single and double-contact phases.

All running trials were completed first. The subjects were instructed to run at a comfortable self-selected pace, aimed towards facilitating a natural running style and a consistent pace between trials, and impact the force plate with their right foot. For the side-cut manoeuvre, the subjects were instructed to perform a slowly paced run-up, impact the centre of the force plate with their right foot, and accelerate to their left-hand side while targeting a cone. The centre of the force plate was marked with white tape and the cone was placed 2 m from the tape mark, angled at 45 degrees from the initial running direction. Backwards running was executed at a self-selected pace, and the subjects had to impact the force plate with their right foot. As the starting position had been established during the practice trials, the subjects only had to focus on executing the movement with consistent technique during measurements, while keeping their focus straight ahead (i.e., away from the running direction). Vertical jump was performed as a counter-movement jump, initiated with the subjects standing with each foot on separate force plates. They were asked to keep their hands fixated on the hips, focus straight ahead for the entirety of the movement cycle, and refrain from excessive hip flexion. While complying with these constraints, they were asked to push-off with their legs at maximal capacity and attempt to achieve their maximal jump height. Finally, ASP was initiated with the subjects' feet separated in the sagittal plane and placed on separate force plates, while their arms were positioned inversely to their feet, closely resembling a natural initiation of running. From this position, they were asked to accelerate to their self-selected running pace. Five trials were completed for all movements, each consisting of one full movement cycle.

2.2 Data collection

35 reflective markers were placed on the subjects, including 29 markers placed on the skin surface and three markers placed on each running shoe at the approximate position of the first and fifth metatarsal and posteriorly on calcaneus. No markers were placed on the head. Further details of the marker protocol are provided as supplementary material. Marker trajectories were tracked using a marker-based motion capture system, consisting of eight infrared high-speed cameras (Oqus 300 series), sampling at 250 Hz, combined with Qualisys Track Manager v. 2.9 (Qualisys, Gothenburg, Sweden). GRF&Ms were obtained at 2000 Hz using two force plates (Advanced Mechanical Technology, Inc., Watertown, MA, US), which were embedded in the laboratory floor.

2.3 Data processing

3-D marker trajectories and force plate data were low-pass filtered using second order, zero-phase Butterworth filters with a cut-off frequency of 15 Hz. For all movements, three of the five successful trials were included for further analysis, yielding a total of 150 trials used to validate the predicted GRF&Ms and the associated joint kinetics. Trials were excluded due to marker occlusion over 10% or inadequate impact of the force plates, meaning that the whole foot was not in contact with the force plate surface or the impact occurred too close to the edges.

2.4 Musculoskeletal model

The musculoskeletal models were developed in the AnyBody Modeling System v. 6.0.4 (AMS) (AnyBody Technology A/S, Aalborg, Denmark) based on the *GaitFullBody* template from the AnyBody Managed Model Repository v. 1.6.3 (Figure 1). In the *GaitFullBody* template, the lower extremity model is based on

the cadaver dataset of Klein Horsman et al. [12], the lumbar spine model based on the work of de Zee et al. [28], and the shoulder and arm models based on the work of the Delft Shoulder Group [29-31]. The model had a total of 39 degrees-of-freedom (DOF), including 2x2 DOF at the ankle joints, 2x1 DOF at the knee joints, 2x3 DOF at the hip joints, 6 DOF at the pelvis, 3 DOF between pelvis and thorax, 2x2 DOF at the elbow joints, 2x5 DOF at the glenohumeral joints, and 2x2 DOF at the wrist joints. As there were no markers placed on the head, the neck joint was fixed in a neutral position.

2.4.1 Geometric and inertial parameter scaling

A length-mass scaling law [32] was applied to scale the musculoskeletal models to the different sizes of the subjects. For the geometric scaling of each segment, a diagonal scaling matrix was applied to each point on the segment. For the longitudinal direction, the entry of the scaling matrix was computed as the ratio between the unscaled and scaled segment lengths. In the two other orthogonal directions, the scaling was computed as the square root of the mass ratios divided by the length ratios between the scaled and unscaled models. The total body mass was distributed to the individual segments by applying the regression equations of Winter et al. [33]. Finally, the inertial parameters were estimated by assuming that the segments were cylindrical with a uniform density and the length and mass equal to the segment length and mass.

2.4.2 Muscle recruitment problem

The muscle recruitment problem was solved by formulating a quadratic optimisation problem, also known as *Quadratic muscle recruitment*, which minimises a scalar objective function, G, subject to the dynamic equilibrium

equations and non-negativity constraints, ensuring that the muscles can only pull and that each unilateral contact element, $f_i^{(C)}$, and pelvis residual force, $f_i^{(R)}$, as will be explained later, can only push. In other words, the sum of the squared muscle, contact, and residual activities (i.e., the ratio between forces and strengths) were minimised to provide the forces. The optimisation problem was formulated as

$$\min_{\mathbf{f}} G(\mathbf{f}^M) = \sum_{i=1}^{n^{(M)}} \left(\frac{f_i^{(M)}}{N_i^{(M)}} \right)^2 + \sum_{i=1}^{5n^{(C)}} \left(\frac{f_i^{(C)}}{N_i^{(C)}} \right)^2 + \sum_{i=1}^{n^{(R)}} \left(\frac{f_i^{(R)}}{N_i^{(R)}} \right)^2 \tag{1}$$

$$\mathbf{Cf} = \mathbf{d}$$

$$0 \leq f_i^{(M)}, \quad i = 1, \dots, n^{(M)},$$

$$0 \leq f_i^{(C)}, \quad i = 1, \dots, 5n^{(C)},$$

$$0 \leq f_i^{(R)}, \quad i = 1, \dots, n^{(R)},$$

where, $f_i^{(M)}$ is the ith muscle force, $n^{(M)}$ is the number of muscles, and $N_i^{(M)}$ is the strength of the muscle. $f_i^{(C)}$ is the ith contact force, $n^{(C)}$ is the number of contact elements, and $N_i^{(C)}$ is the strength of the contact element. $f_i^{(R)}$ is the ith residual force, $n^{(R)}$ is the number of residual forces, and $N_i^{(R)}$ is the strength of the residual force. $\mathbf{C}$ is the coefficient matrix for the dynamic equilibrium equations, $\mathbf{f}$ is a vector of unknown muscle, joint reaction, contact, and residual forces, and $\mathbf{d}$ contains all external loads and inertia forces. Further details can be found in Damsgaard et al. [8].

The muscle strengths were based on the datasets for the different body parts and assumed constant, meaning that the maximum muscle forces were kept constant for all muscle states (e.g., muscle length and contraction velocity), and adjusted using a strength scaling factor based on fat percentage [30], which was

estimated from each subject's Body-Mass-Index using the regression equations reported by Frankenfield et al. [34].

The lower extremity model included a total of 110 muscles, divided into 318 individual muscle paths, whereas ideal joint torque generators were used for the upper extremities. In addition, residual force actuators were added to the origin of the pelvis segment, which were able to generate residual forces and moments up to 10 N or Nm. The activation levels of these actuators were solved as part of the muscle recruitment, aimed towards minimising their contribution.

2.4.3 Model scaling and kinematics

Model scaling and kinematic analysis were performed applying the optimisation methods of Andersen et al. [10, 35]. During the experiment, the subjects performed multiple gait trials of which a single trial for each subject was initially used to determine segment lengths and model marker positions. These parameters were estimated by minimising the least-square difference between model and experimental markers using the method of Andersen et al. [35]. For each subject, the segment lengths and marker positions obtained from the gait trial were subsequently saved and used for the analysis of all other trials. Specifically, the optimised parameters were loaded and the least-square difference between model and experimental markers minimised over the whole trial duration to obtain the model kinematics [10]. Further details regarding the marker optimisation procedure is provided as supplementary material.

2.5 Prediction of GRF&Ms

The prediction of the GRF&Ms was enabled by adopting the method of Fluit et al. [19]. However, some alterations were made to adjust for the different conditions in

12

the present study as well as improving the method's ease of implementation, which are specified in the following. The GRF&Ms were predicted by creating contact elements at 18 points defined under each foot of the musculoskeletal model (Figure 2). In order to compensate for the sole thickness of the running shoes and the soft tissue under the heel, the contact points on the heel were offset by 35 mm and all other points offset by 25 mm from the model bone geometry. Each contact element consisted of five unilateral force actuators organised to approximate a static Coulomb friction model; one actuator was aligned with the vertical axis of the force plates (Z-axis), and generated a normal force, while the other four actuators were defined in two pairs that were aligned with the medio-lateral (X-axis) and antero-posterior axis (Y-axis) of the force plates, and were able to generate positive and negative static friction forces (with a friction coefficient of 0.5). The four shear actuators were organised such that they independently were able to generate a force in the normal direction and in one of the four shear directions (positive or negative medial-lateral direction or positive or negative antero-posterior direction). For each of these four, the forces were defined such that if they were actuated to generate a force, F_n, in the normal direction, they would at the same time generate a force of μF_n in the shear direction, where μ is the friction coefficient. Hereby, the total normal force at a contact point is equal to the sum of the five normal forces and the magnitude of the friction force is bounded by the normal force.

To accommodate the fact that there can only be contact forces at the contact points when they are close to the ground plane and stationary, a strength factor, similar to the one used for muscles, was introduced and the magnitudes of the predicted GRF&Ms were determined by solving the activation level of

muscle, joint, and ground contact forces as part of the muscle recruitment algorithm simultaneously.

The strength factor ensured that the contact elements would only generate forces if their associated contact point, p, was sufficiently close to the floor and almost without motion. Furthermore, in order to be activated, each contact point had to overlap with a user-defined artificial ground plane in the model environment, as illustrated in Figure 2. The maximal strength of each actuator was set to $N_{\max} = 0.4$ BW, the activation threshold distance for p was set to $z_{limit} = 0.04$ m, and the activation threshold velocity of p relative to the ground plane was set to $v_{\mathrm{limit}} = 1.3$ m/s. The threshold distance, z_{limit}, specifies the location of the artificial ground plane relative to the origin of the global reference frame and not the actual location of the ground. The maximal strength of the actuators and the threshold velocity were similar to the values used in Fluit et al. [19], while the threshold distance and muscle recruitment criterion were determined by performing multiple simulations of a single gait trial for each participant and adjusting these parameters to obtain the most accurate results. The chosen threshold distance and muscle recruitment criterion were then used for all other trials.

To determine the strength profile of each contact point, a nonlinear strength function was defined:

$$c_{p,i} = \begin{cases} N_{\max} & \text{if} \quad z_{\mathrm{ratio}} \leq 0.8 \text{ and } v_{\mathrm{ratio}} \leq 0.15 \\ N_{\mathrm{smooth}} & \text{if} \quad 0.8 \leq z_{\mathrm{ratio}} < 1 \text{ and } 0.15 \leq v_{\mathrm{ratio}} < 1 \\ 0 & \text{otherwise} \end{cases} \quad (2)$$

$$\text{where} \quad z_{\mathrm{ratio}} = \frac{p_{\mathrm{z}}}{z_{\mathrm{limit}}}$$

$$\text{and} \quad v_{\mathrm{ratio}} = \frac{p_{\mathrm{vel}}}{v_{\mathrm{limit}}}$$

p_z and p_{vel} defined the height and velocity of each contact point relative to the ground, respectively. Eq. (2) specifies that each actuator would assume the strength N_{max} if the associated p reached z_{limit} and v_{limit}. However, in order to prevent discontinuities in the predicted GRF&Ms due to the sudden transition of p from inactive to fully active, a smoothing function was defined:

$$N_{smooth} = N_{max} z_{smooth} v_{smooth} \qquad (3)$$

$$\text{where} \quad z_{smooth} = 0.5 \left(\cos \left(\frac{z_{ratio} - 0.8}{(1 - 0.8)\pi} \right) + 1 \right)$$

$$\text{and} \quad v_{smooth} = 0.5 \left(\cos \left(\frac{v_{ratio} - 0.15}{(1 - 0.15)\pi} \right) + 1 \right)$$

The smoothing function would be assumed when p was near z_{limit} and v_{limit}, as specified in Eq. (2); hence, the strength of the actuators would build up gradually until the threshold values were reached.

During muscle recruitment, the forces of the skeletal muscles and the contact elements were weighted equally, but the strength of the contact element forces was high compared to the skeletal muscles, whereas the strength of the residual forces and moments placed on the pelvis was relatively low. This means that the actuation of the contact elements, when in full contact with the ground, were of practically no cost in the objective function, which enabled the recruitment algorithm to distribute the contact forces such that the muscle loads were minimised. The solver did not distinguish between single and double-support phases, hereby, providing a solution to the problem of under-determinacy.

2.6 Data Analysis

For the running, backwards running, and side-cut trials, data were analysed from the first foot-force plate contact instant to the last frame of contact. Vertical jump

trials were analysed in the 800 ms up till toe-off, which included the complete counter-movement cycle. ASP trials were analysed in the 600 ms up till toe-off of the rear foot. The following variables were included in the analysis: antero-posterior GRF, medio-lateral GRF, vertical GRF, sagittal ground reaction moment (GRM), frontal GRM, transverse GRM, ankle flexion moment (AFM), ankle subtalar eversion moment (ASEM), knee flexion moment (KFM), hip flexion moment (HFM), hip abduction moment (HAM), hip external rotation moment (HERM), ankle resultant joint reaction force (JRF), knee resultant JRF, and hip resultant JRF. In addition, peak vertical GRFs and peak resultant JRFs for the ankle, knee, and hip were computed and statistically compared. For the running, backwards running, and side-cut trials, the selected variables were analysed for the right leg only, i.e., the stance phases of the movement cycles. For the vertical jump and ASP trials, the variables were analysed for the right and left leg separately.

Pearson's correlation coefficient (r) and root-mean-square deviation (RMSD) were computed to compare the shape and magnitude, respectively, of the selected variables between the models. Following the procedures of Taylor [36], the absolute values of r were categorized as weak, moderate, strong, and excellent for $r \leq 0.35$, $0.35 < r \leq 0.67$, $0.67 < r \leq 0.90$, and $0.90 < r$, respectively. To test the differences between the computed peak GRFs and peak resultant JRFs associated with each method, Wilcoxon paired-sample tests were applied for which $p < 0.05$ are reported as a significant difference.

3. Results

The time-histories of the selected variables for running, backwards running, and side-cut are depicted in Figures 3-7 (a), and vertical jump and ASP trials are

depicted in Figures 3-7 (b). Specifically, the GRFs are depicted in Figure 3 (a, b), GRMs in Figure 4 (a, b), joint moments in Figure 5 and 6 (a, b), and JRFs in Figure 7 (a, b). Pearson's correlation coefficients and RMSD are listed in Tables 1 and 2 (a) for running, backwards running, and side-cut, and in Tables 1 and 2 (b) for vertical jump and ASP. The results of the Wilcoxon-paired sample tests are listed in Table 3.

Across all movements, excellent correlations were found for the vertical GRF (r ranging from 0.96 to 0.99, median 0.99), and strong to excellent correlations were found for the sagittal GRM (r ranging from 0.69 to 0.95, median 0.87), all joint flexion moments (r ranging from 0.79 to 0.98, median 0.93), and resultant JRFs (r ranging from 0.78 to 0.99, median 0.97). The variables showing the largest discrepancies between datasets were the transverse GRM (r ranging from -0.19 to 0.86, median 0.09), frontal GRM (r ranging from 0.39 to 0.96, median 0.59), and medio-lateral GRF (r ranging from 0.13 to 0.96, median 0.61). The RMSD showed that the magnitude differences were generally low, ranging from 1.88 to 16.68 (% BW), median 6.75, for the GRFs, 0.50 to 3.46 (% BW BH), median 1.17, for the GRMs, 0.41 to 3.73, median 1.26, for the joint moments, and 33.02 to 177.49, median 72.43, for the JRFs. However, the model overestimated the majority of the peak forces, and the Wilcoxon-paired sample tests showed significant differences for 21 of the 28 computed variables. No significant differences were found for the peak vertical GRF for both the right (RL) (p = 0.1156) and left leg (LL) (p = 0.0978) during ASP, ankle peak resultant JRF during side-cut (p = 0.6143), knee peak resultant JRF during backwards running (p = 0.8444) and for the RL (p = 0.5720) and LL (p = 0.2149) during vertical jump, and hip peak resultant JRF (0.0519) for the RL during ASP. The results for each movement are summarised in the following.

3.1 Running

For the GRF&Ms during running, strong to excellent correlations, see Table 1 (a), were observed for all variables of notable magnitude, including the vertical GRF (0.99 ± 0.00), antero-posterior GRF (0.88 ± 0.12), and sagittal GRM (0.87 ± 0.09), whereas the forces and moments of relatively small magnitude showed weak to moderate correlations, specifically the medio-lateral GRF (0.13 ± 0.37), frontal GRM (0.50 ± 0.24), and transverse GRM (-0.04 ± 0.33). Overall, the model provided comparable estimates of joint kinetics, showing strong to excellent correlations for all joint moments (r ranging from 0.71 to 0.92, median 0.87) and resultant JRFs (r ranging from 0.93 to 0.98). The RMSD, see Table 2 (a), ranged from 5.50 to 15.09 for the GRFs, 1.17 to 3.59 for the GRMs, 1.17 to 3.31 for the joint moments, and 74.92 to 177.49 for the JRFs.

3.2 Backwards running

Similar to running, the results for backwards running showed strong to excellent correlations, see Table 1 (a), for the vertical GRF (0.99 ± 0.00), antero-posterior GRF (0.94 ± 0.02), and sagittal GRM (0.88 ± 0.09), whereas weak to moderate correlations were found for the medio-lateral GRF (0.53 ± 0.28), frontal GRM (0.39 ± 0.34), and transverse GRM (0.09 ± 0.34). Furthermore, strong to excellent correlations were found for all joint moments (r ranging from 0.68 to 0.94, median 0.87) and resultant JRFs (r ranging from 0.84 to 0.98). The RMSD, see Table 2 (a), ranged from 4.64 to 12.82 for the GRFs, 0.89 to 2.94 for the GRMs, 0.88 to 2.57 for the joint moments, and 62.70 to 147.56 for the JRFs.

3.3 Side-cut

Compared to the two running activities, the medio-lateral GRF and transverse GRM were of considerably higher magnitude during side-cut, resulting in correlation coefficients, see Table 1 (a), of 0.96 ± 0.02 and 0.86 ± 0.09, respectively. Otherwise, similar results were found for the vertical GRF (0.97 ± 0.02), antero-posterior GRF (0.89 ± 0.12), frontal GRM (0.58 ± 0.30), and sagittal GRM (0.79 ± 0.09). Joint flexion moments (r ranging from 0.79 to 0.94) and resultant JRFs (r ranging from 0.83 to 0.95) showed strong to excellent correlations. The RMSD, see Table 2 (a), ranged from 8.70 to 16.68 for the GRFs, 1.65 to 3.46 for the GRMs, 1.68 to 3.73 for the joint moments, and 87.97 to 172.68 for the JRFs.

3.4 Vertical jump

For vertical jump, the majority of the variables showed comparable results between the models, and similar results for the RL and LL, highlighted by the strong to excellent correlations, see Table 1 (b), found for the vertical GRFs (0.98 ± 0.01), medio-lateral GRFs (RL: 0.82 ± 0.13, LL: 0.86 ± 0.08), frontal GRMs (RL: 0.96 ± 0.00, LL: 0.96 ± 0.02), sagittal GRMs (RL: 0.92 ± 0.08, LL: 0.87 ± 0.12), joint flexion moments (r ranging from 0.95 to 0.98, median 0.96), ankle subtalar eversion moments (RL: 0.93 ± 0.04, LL: 0.87 ± 0.10), and resultant JRFs (r ranging from 0.97 to 0.99, median 0.99). Weak to strong correlations were found for the remaining variables (r ranging from -0.13 to 0.78, median 0.59), for which, however, the forces and moments were of considerably lower magnitude. The RMSD, see Table 2 (b), ranged from 2.05 to 7.03 for the GRFs, 0.50 to 1.32 for the GRMs, 0.41 to 1.54 for the joint moments, and 33.02 to 72.43 for the JRFs.

3.5 ASP

Compared to vertical jump, ASP involved different movement patterns for each leg, leading to different characteristics in the kinetic data. However, the statistical results were similar between legs for the majority of the variables with the main findings being the excellent correlations, see Table 1 (b), for the vertical GRFs (0.99 ± 0.01) and antero-posterior GRFs (RL: 0.97 ± 0.02, LL: 0.99 ± 0.01), and the strong to excellent correlations found for all joint moments (r ranging from 0.77 to 0.98, median 0.90) and resultant JRFs (r ranging from 0.78 to 0.99, median 0.94). The most notable differences between the variables associated with each leg were the frontal (RL: 0.83 ± 0.12, LL: 0.47 ± 0.37) and sagittal GRM (RL: 0.69 ± 0.14, LL: 0.95 ± 0.03). The RMSD, see Table 2 (b), ranged from 1.88 to 9.62 for the GRFs, 0.51 to 1.76 for the GRMs, 0.39 to 1.45 for the joint moments, and 49.09 to 92.91 for the JRFs.

4. Discussion

In this study, the method of Fluit et al. [19] to predict GRF&Ms was adopted and validated for an array of movements associated with sports and recreational exercise. Alterations were made to the original method, which included the implementation of a new smoothing function and additional contact points to the dynamic contact model. The predicted GRF&Ms and associated joint kinetics were compared to the corresponding variables obtained from a model, where a traditional IDA was applied, in which the GRF&Ms were measured using force plates.

      The main findings were that the model was able to provide estimates comparable to the traditional IDA approach for the vertical GRFs, joint flexion

moments, and resultant JRFs based on the strong to excellent correlations found for all these variables and the generally low magnitude differences. These results were, furthermore, overall similar between movements involving only single contact phases (e.g., running), entirely double contact (vertical jump), and a transition from double to single contact (ASP). The results for the GRMs, antero-posterior GRFs, and medio-lateral GRFs varied between movements and discrepancies were identified, particularly for the transverse and frontal GRMs. Finally, despite the overall shape and magnitude similarities in the datasets, the computed peak vertical GRFs and resultant JRFs showed discrepancies, and significant differences were found for the majority of these variables.

The discrepancies found for the medio-lateral GRFs, frontal GRMs, and transverse GRMs can likely be explained by the low magnitude of these variables, which increased the influence of noise. When these variables increased in magnitude, the correlations between datasets likewise increased, such as the frontal GRM during vertical jump ($r = 0.96 \pm 0.02$) and transverse GRM during side-cut ($r = 0.86 \pm 0.09$). This tendency indicates that the low signal-to-noise ratio was the predominant issue for these inaccuracies. It also shows that the correlation coefficient might not be an appropriate tool to compare variables of such low magnitudes, as the results can be misleading.

The transverse GRMs showed the lowest correlations between datasets, which was consistent with the findings of Fluit et al. [19]. This result could be partly caused by the constraint imposed by the simplified model of the knee as a hinge-joint, which did not allow for transversal rotation. This issue could, furthermore, have caused the relatively poor agreement of the HERM for the majority of the movements. Therefore, future studies could advantageously

21

implement a knee model with a more detailed geometry or an advanced knee model, as for instance the model proposed by Marra et al. [37].

In order to improve the model's prediction of GRF&Ms, a number of parameters could be adjusted in the dynamic contact model. First, the contact point offsets were approximated, considering the sole thickness of the running shoes and the soft tissue under the heel, and measurements of these parameters could possibly improve the ground contact determination. However, the points are required to overlap with the artificial ground plane in the model environment and have to be adjusted accordingly. Second, the number and position of the contact points could be adjusted to provide more detailed modelling of the foot-ground contact, accounting for the underside characteristics of the foot or specific footwear used. Third, a sensitivity analysis could have been performed on the contact parameters, N_{max}, z_{limit}, and v_{limit}, as well as the threshold values for z_{ratio} and v_{ratio}, hereby, determining a set of optimal values. This could potentially have reduced the overestimations of peak forces that were identified for the majority of the analysed variables, and represented the clearest discrepancy between datasets. Future studies could advantageously deploy a sensitivity analysis involving all or several of the contact parameters to find an optimal combination, aimed towards achieving the highest possible accuracy in the model estimates.

A number of limitations should be noted. First, it is well-known that marker trajectories are associated with noise, especially due to soft-tissue artefacts [38], and methods to sufficiently compensate for these inaccuracies does currently not exist [39]. Second, the foot was modelled as a single segment, and the dynamic contact model could have been improved by applying a multi-segment foot model. In particular, a model that enables bending of the toes would likely

increase the accuracy of the predictions around toe-off. Third, the muscle models did not incorporate contraction dynamics, e.g., as modelled with a Hill-type muscle model, which might have altered the model kinetics, including the predicted GRF&Ms. However, this would require the determination of additional individual parameters, such as passive stiffness, tendon slack length, optimal fiber length etc., which are typically estimated through calibration procedures and are also sources of uncertainty in the model. Furthermore, incorporating muscle contraction dynamics would most likely only have any influence on the variables of interest during ASP, since it is an asymmetrical double-supported movement.

The presented method provides a number of valuable opportunities for future studies, particularly within sports science research. By obviating the need for force plate measurements, this method facilitates the analysis of sports-related movements that occupy a large space or can only be analysed in their entirety in outdoor environments, and excludes the potential influence of force plate targeting. Another potential benefit is that the method enables the determination of GRF&Ms in situations, where force plates are difficult and expensive to instrument, such as motion analysis during treadmill walking or running. Finally, an exciting perspective is the combination of the method with motion analysis systems that do not commonly incorporate an interface between kinematic and force plate data, such as miniature inertial sensors [40] or marker-less motion capture [41]. Recently, Skals et al. [42] introduced an interface between marker-less motion capture data and a musculoskeletal model, thus providing the first step towards complete IDA using such systems.

Prediction of GRF&Ms can reduce dynamic inconsistency and obviate the need for force plate measurements when performing IDA of musculoskeletal models. This study provided validation of a method to predict GRF&Ms from

full-body motion only for an array of sports-related movements. The method provided estimates comparable to traditional IDA for the majority of the analysed variables, including vertical GRFs, joint flexion moments, and resultant JRFs. Based on these results, the method could be used instead of force plate data, hereby, facilitating the analysis of sports-related movements and providing new opportunities for complete IDA using systems that do not provide an interface between kinematic and force plate data.

Conflict of Interest:

M. Damsgaard is head of development, minority shareholder, and member of the board of directors of AnyBody Technology A/S that owns and sells the AnyBody Modeling System.

5. References

1. Zajac, F.E., Neptune, R.R., Kautz, S.A.: Biomechanics and muscle coordination of human walking: Part I: Introduction to concepts, power transfer, dynamics and simulations. Gait Posture **16**(3), 215-232 (2002).

2. Rasmussen, J., Damsgaard, M., Surma, E., Christensen, S.T., de Zee, M., Vondrak, V.: Anybody-a software system for ergonomic optimization. In: Abstracts of the Fifth World Congress on Structural and Multidisciplinary Optimization, Lido di Jesolo, Venice, Italy, 19-23 May 2003

3. Mellon, S.J., Grammatopoulos, G., Andersen, M.S., Pandit, H.G., Gill, H.S., Murray, D.W.: Optimal acetabular component orientation estimated using edge-loading and impingement risk in patients with metal-on-metal hip resurfacing arthroplasty. J. Biomech. **48**(2), 318-323 (2015).

4. Payton, C., Bartlett, R.: Biomechanical evaluation of movement in sport and exercise: the British Association of Sport and Exercise Sciences guide. Routledge, Abingdon (2007)

5. Thelen, D.G., Anderson, F.C.: Using computed muscle control to generate forward dynamic simulations of human walking from experimental data. J. Biomech. **39**(6), 1107-1115 (2006).

6. Barrett, R.S., Besier, T.F., Lloyd, D.G.: Individual muscle contributions to the swing phase of gait: An EMG-based forward dynamics modelling approach. Simul. Model. Pract. Th. **15**(9), 1146-1155 (2007).

7. Anderson, F.C., Pandy, M.G.: Dynamic optimization of human walking. J. Biomech. Eng. **123**(5), 381-390 (2001).

8. Damsgaard, M., Rasmussen, J., Christensen, S.T., Surma, E., de Zee, M.: Analysis of musculoskeletal systems in the AnyBody Modeling System. Simul. Model. Pract. Th. **14**(8), 1100-1111 (2006).

9. Rasmussen, J., Damsgaard, M., Voigt, M.: Muscle recruitment by the min/max criterion—a comparative numerical study. J. Biomech. **34**(3), 409-415 (2001).

10. Andersen, M.S., Damsgaard, M., Rasmussen, J.: Kinematic analysis of over-determinate biomechanical systems. Comput. Methods Biomech. Biomed. Engin. **12**(4), 371-384 (2009).

11. Psycharakis, S.G., Miller, S.: Estimation of errors in force platform data. Res. Q. Exerc. Sport **77**(4), 514-518 (2006).

12. Klein Horsman, M.D., Koopman, H.F.J.M., Van der Helm, F.C.T., Prosé, L.P., Veeger, H.E.J.: Morphological muscle and joint parameters for musculoskeletal modelling of the lower extremity. Clin. Biomech. **22**(2), 239-247 (2007).

13. Lund, M.E., Andersen, M.S., de Zee, M., Rasmussen, J.: Scaling of musculoskeletal models from static and dynamic trials. Int. Biomech. **2**(1), 1-11 (2015).

14. Pàmies-Vila, R., Font-Llagunes, J.M., Cuadrado, J., Javier Alonso, F.: Analysis of different uncertainties in the inverse dynamic analysis of human gait. Mech. Mach. Theory **58**, 153-164 (2012).

15. Riemer, R., Hsiao-Wecksler, E.T., Zhang, X.: Uncertainties in inverse dynamics solutions: A comprehensive analysis and an application to gait. Gait Posture **27**(4), 578–588 (2008).

16. Hatze, H.: The fundamental problem of myoskeletal inverse dynamics and its implications. J. Biomech. **35**(1), 109-115 (2002).

17. Cahouët, V., Luc, M., David, A.: Static optimal estimation of joint accelerations for inverse dynamics problem solution. J. Biomech. **35**(11), 1507-1513 (2002).

18. Kuo, A.D.: A least-squares estimation approach to improving the precision of inverse dynamics computations. J. Biomech. Eng. **120**(1), 148-159 (1998).

19. Fluit, R., Andersen, M.S., Kolk, S., Verdonschot, N., Koopman, H.: Prediction of ground reaction forces and moments during various activities of daily living. J. Biomech. **47**(10), 2321-2329 (2014).

20. Riemer, R., Hsiao-Wecksler, E.T.: Improving joint torque calculations: Optimization-based inverse dynamics to reduce the effect of motion errors. J. Biomech. **41**(7), 1503-1509 (2008).

21. Audu, M.L., Kirsch, R.F., Triolo, R.J.: Experimental verification of a computational technique for determining ground reactions in human bipedal stance. J. Biomech. **40**(5), 1115-1124 (2007).

22. Choi, A., Lee, J.-M., Mun, J.H.: Ground reaction forces predicted by using artificial neural network during asymmetric movements. Int. J. Precis. Eng. Manuf. **14**(3), 475-483 (2013).

23. Robert, T., Causse, J., Monnier, G.: Estimation of external contact loads using an inverse dynamics and optimization approach: general method and application to sit-to-stand maneuvers. J. Biomech. **46**(13), 2220-2227 (2013).

24. Ren, L., Jones, R.K., Howard, D.: Whole body inverse dynamics over a complete gait cycle based only on measured kinematics. J. Biomech. **41**(12), 2750-2759 (2008).

25. Lugrís, U., Carlín, J., Pàmies-Vilà, R., Font-Llagunes, M., Cuadrado, J.: Solution methods for the double-support indeterminacy in human gait. Multibody Syst. Dyn. **30**(3), 247-263 (2013).

26. Jackson, J.N., Hass, C.J., Fregly, B.J.: Development of a subject-specific foot-ground contact model for walking. J. Biomech. Eng. **138**(9), 091002 (2016).

27. Challis, J.H.: The variability in running gait caused by force plate targeting. J. Appl. Biomech. **17**(1), 77-83 (2001).

28. De Zee, M., Hansen, L., Wong, C., Rasmussen, J., Simonsen, E.B.: A generic detailed rigid-body lumbar spine model. J. Biomech. **40**(6), 1219-1227 (2007).

29. Veeger, H.E.J., Van der Helm, F.C.T., Van der Woude, L.H.V., Pronk, G.M., Rozendal, R.H.: Inertia and muscle contraction parameters for musculoskeletal modelling of the shoulder mechanism. J. Biomech. **24**(7), 615-629 (1991).

30. Veeger, H.E.J., Yu, B., An, K.-N., Rozendal, R.H.: Parameters for modeling the upper extremity. J. Biomech. **30**(6), 647-652 (1997).

31. Van der Helm, F.C., Veeger, H., Pronk, G., Van der Woude, L., Rozendal, R.: Geometry parameters for musculoskeletal modelling of the shoulder system. J. Biomech. **25**(2), 129-144 (1992).

32. Rasmussen, J., Zee, M.d., Damsgaard, M., Christensen, S.T., Marek, C., Siebertz, K.: A general method for scaling musculo-skeletal models. Paper presented at the 10th international symposium on computer simulation in biomechanics, Case Western Reserve University, Cleveland, USA, 28-30 July 2005

33. Winter, D.A.: Biomechanics and motor control of human movement, 4th edition. John Wiley & Sons, Hoboken (2009)

34. Frankenfield, D.C., Rowe, W.A., Cooney, R.N., Smith, J.S., Becker, D.: Limits of body mass index to detect obesity and predict body composition. Nutrition **17**(1), 26-30 (2001).

35. Andersen, M.S., Damsgaard, M., MacWilliams, B., Rasmussen, J.: A computationally efficient optimisation-based method for parameter identification of kinematically determinate and over-determinate biomechanical systems. Comput. Methods Biomech. Biomed. Engin. **13**(2), 171-183 (2010).

36. Taylor, R.: Interpretation of the correlation coefficient: a basic review. J. Diagn. Med. Sonog. **6**(1), 35-39 (1990).

37. Marra, M.A., Vanheule, V., Fluit, R., Koopman, B.H., Rasmussen, J., Verdonschot, N., Andersen, M.S.: A subject-specific musculoskeletal modeling framework to predict in vivo mechanics of total knee arthroplasty. J. Biomech. Eng. **137**(2), 020904 (2015).

38. Leardini, A., Chiari, L., Della Croce, U., Cappozzo, A.: Human movement analysis using stereophotogrammetry: Part 3. Soft tissue artifact assessment and compensation. Gait Posture **21**(2), 212-225 (2005).

39. Benoit, D.L., Damsgaard, M., Andersen, M.S.: Surface marker cluster translation, rotation, scaling and deformation: Their contribution to soft tissue artefact and impact on knee joint kinematics. J. Biomech. **48**(10), 2124-2129 (2015).

40. Roetenberg, D., Luinge, H., Slycke, P.: Xsens MVN: full 6DOF human motion tracking using miniature inertial sensors. Xsens Motion Technologies BV, Tech. Rep (2009).

41. Sandau, M., Koblauch, H., Moeslund, T.B., Aanæs, H., Alkjær, T., Simonsen, E.B.: Markerless motion capture can provide reliable 3D gait kinematics in the sagittal and frontal plane. Med. Eng. Phys. **36**(9), 1168-1175 (2014).

42. Skals, S., Rasmussen, K., Bendtsen, K., Andersen, M.S.: Validation of musculoskeletal models driven by dual Microsoft Kinect Sensor data. In: Abstracts of the 13th International Symposium on 3D analysis of Human Movement, Lausanne, Switzerland, 14-17 July 2014

Table 1 (a) - Pearson's correlation coefficients for the selected variables during running, backwards running, and side-cut. The results are presented as the mean ± 1 SD.

Variable	Running	Backwards running	Side-cut
Antero-posterior GRF	0.88 ± 0.12	0.94 ± 0.02	0.89 ± 0.12
Medio-lateral GRF	0.13 ± 0.37	0.53 ± 0.28	0.96 ± 0.02
Vertical GRF	0.99 ± 0.00	0.99 ± 0.00	0.97 ± 0.02
Frontal GRM	0.50 ± 0.24	0.39 ± 0.34	0.58 ± 0.30
Sagittal GRM	0.87 ± 0.09	0.88 ± 0.09	0.79 ± 0.09
Transverse GRM	-0.04 ± 0.33	0.09 ± 0.34	0.86 ± 0.09
AFM	0.89 ± 0.07	0.89 ± 0.09	0.79 ± 0.10
ASEM	0.71 ± 0.12	0.70 ± 0.15	0.47 ± 0.36
KFM	0.92 ± 0.05	0.94 ± 0.05	0.94 ± 0.09
HFM	0.85 ± 0.05	0.88 ± 0.06	0.92 ± 0.05
HAM	0.90 ± 0.10	0.85 ± 0.14	0.37 ± 0.37
HERM	0.72 ± 0.21	0.68 ± 0.31	0.62 ± 0.22
Ankle resultant JRF	0.93 ± 0.04	0.93 ± 0.05	0.87 ± 0.12
Knee resultant JRF	0.98 ± 0.01	0.98 ± 0.01	0.95 ± 0.04
Hip resultant JRF	0.94 ± 0.05	0.84 ± 0.14	0.83 ± 0.13

Table 1 (b) - Pearson's correlation coefficients for the selected variables during vertical jump and acceleration from a standing position (ASP). The results are presented as the mean ± 1 SD.

Variable	Vertical jump Right leg	Vertical jump Left leg	ASP Right leg	ASP Left leg
Antero-posterior GRF	0.63 ± 0.28	0.68 ± 0.25	0.97 ± 0.02	0.99 ± 0.01
Medio-lateral GRF	0.82 ± 0.13	0.86 ± 0.08	0.61 ± 0.27	0.59 ± 0.37
Vertical GRF	0.98 ± 0.01	0.98 ± 0.01	0.99 ± 0.01	0.99 ± 0.01
Frontal GRM	0.96 ± 0.00	0.96 ± 0.02	0.83 ± 0.12	0.47 ± 0.37
Sagittal GRM	0.92 ± 0.08	0.87 ± 0.12	0.69 ± 0.14	0.95 ± 0.03
Transverse GRM	-0.13 ± 0.39	-0.19 ± 0.47	0.77 ± 0.17	0.60 ± 0.27
AFM	0.96 ± 0.02	0.96 ± 0.02	0.88 ± 0.07	0.98 ± 0.01
ASEM	0.93 ± 0.04	0.87 ± 0.10	0.83 ± 0.10	0.86 ± 0.10
KFM	0.95 ± 0.03	0.95 ± 0.03	0.86 ± 0.08	0.92 ± 0.06
HFM	0.98 ± 0.01	0.98 ± 0.01	0.93 ± 0.06	0.97 ± 0.02
HAM	0.78 ± 0.18	0.72 ± 0.26	0.92 ± 0.06	0.87 ± 0.10
HERM	0.51 ± 0.39	0.55 ± 0.34	0.93 ± 0.05	0.77 ± 0.14
Ankle resultant JRF	0.97 ± 0.02	0.97 ± 0.01	0.91 ± 0.06	0.98 ± 0.01
Knee resultant JRF	0.99 ± 0.01	0.99 ± 0.01	0.88 ± 0.07	0.99 ± 0.01
Hip resultant JRF	0.99 ± 0.01	0.99 ± 0.00	0.78 ± 0.14	0.97 ± 0.04

Table 2 (a) – RMSD for the selected variables during running, backwards running, and side-cut.

The results are presented as the mean ± 1 SD.

Variable	Running	Backwards running	Side-cut
Antero-posterior GRF (% BW)	7.77 ± 3.58	6.75 ± 1.37	12.86 ± 3.88
Medio-lateral GRF (% BW)	5.50 ± 1.49	4.64 ± 1.28	8.70 ± 1.58
Vertical GRF (% BW)	15.09 ± 3.45	12.82 ± 3.71	16.68 ± 3.97
Frontal GRM (% BW BH)	1.74 ± 0.43	1.61 ± 0.43	1.65 ± 0.50
Sagittal GRM (% BW BH)	3.59 ± 1.50	2.94 ± 1.00	3.46 ± 0.94
Transverse GRM (% BW BH)	1.17 ± 0.32	0.89 ± 0.32	2.75 ± 0.52
AFM (% BW BH)	3.31 ± 1.15	2.57 ± 1.01	3.73 ± 0.94
ASEM (% BW BH)	1.41 ± 0.38	1.21 ± 0.22	1.68 ± 0.45
KFM (% BW BH)	2.15 ± 0.56	1.58 ± 0.56	2.33 ± 1.36
HFM (% BW BH)	2.72 ± 0.88	2.22 ± 0.48	3.48 ± 1.89
HAM (% BW BH)	1.49 ± 0.44	1.37 ± 0.43	2.74 ± 0.78
HERM (% BW BH)	1.17 ± 0.32	0.88 ± 0.32	2.72 ± 0.69
Ankle resultant JRF (% BW)	177.49 ± 63.00	147.56 ± 55.69	172.68 ± 54.29
Knee resultant JRF (% BW)	74.92 ± 22.47	62.70 ± 14.74	87.97 ± 28.61
Hip resultant JRF (% BW)	100.31 ± 23.37	99.07 ± 20.71	134.93 ± 69.68

Table 2 (b) – RMSD for the selected variables during vertical jump and acceleration from a standing position (ASP). The results are presented as the mean ± 1 SD.

Variable	Vertical jump Right leg	Vertical jump Left leg	ASP Right leg	ASP Left leg
Antero-posterior GRF (% BW)	4.57 ± 1.61	4.45 ± 1.52	3.45 ± 1.24	3.91 ± 1.17
Medio-lateral GRF (% BW)	2.18 ± 0.60	2.05 ± 0.54	1.88 ± 0.74	2.97 ± 1.12
Vertical GRF (% BW)	6.99 ± 1.38	7.03 ± 2.06	6.99 ± 2.17	9.62 ± 1.92
Frontal GRM (% BW BH)	1.32 ± 0.28	1.27 ± 0.35	0.51 ± 0.19	0.93 ± 0.13
Sagittal GRM (% BW BH)	0.50 ± 0.19	0.61 ± 0.22	1.76 ± 0.38	1.15 ± 0.24
Transverse GRM (% BW BH)	0.93 ± 0.35	1.07 ± 0.39	0.57 ± 0.17	0.94 ± 0.19
AFM (% BW BH)	1.07 ± 0.24	1.03 ± 0.27	1.35 ± 0.29	1.11 ± 0.31
ASEM (% BW BH)	0.41 ± 0.15	0.41 ± 0.11	0.39 ± 0.10	0.63 ± 0.12
KFM (% BW BH)	1.23 ± 0.29	1.23 ± 0.24	0.91 ± 0.32	1.00 ± 0.30
HFM (% BW BH)	1.29 ± 0.42	1.30 ± 0.36	0.96 ± 0.45	1.45 ± 0.54
HAM (% BW BH)	0.73 ± 0.18	0.70 ± 0.17	0.72 ± 0.33	0.87 ± 0.30
HERM (% BW BH)	1.54 ± 0.71	1.44 ± 0.65	0.40 ± 0.18	0.95 ± 0.53
Ankle resultant JRF (% BW)	70.80 ± 17.75	72.43 ± 18.75	92.91 ± 21.83	74.26 ± 24.16
Knee resultant JRF (% BW)	33.02 ± 5.66	34.63 ± 11.79	67.32 ± 24.16	49.09 ± 13.91
Hip resultant JRF (% BW)	35.70 ± 10.32	38.05 ± 14.47	57.02 ± 18.42	57.97 ± 22.64

Table 3 – Results of the Wilcoxon paired-sample tests, listing the mean difference ± 1 SD between peak forces. Significant differences are indicated with a *.

Movement	Peak vertical GRF (% BW)	Ankle peak resultant JRF (% BW)	Knee peak resultant JRF (% BW)	Hip peak resultant JRF (% BW)
Running	-14.15 ± 6.89*	-270.03 ± 204.17*	-111.38 ± 66.34*	-144.53 ± 68.60*
Backwards running	-13.89 ± 9.17*	-155.22 ± 138.80*	-54.28 ± 54.00	-79.90 ± 59.62*
Side-cut	-16.19 ± 7.88*	11.44 ± 142.18	-40.97 ± 80.71*	7.14 ± 265.39*
Vertical jump (Right leg)	-6.26 ± 5.21*	-127.79 ± 67.18*	-35.24 ± 39.19	-23.56 ± 46.69*
Vertical jump (Left leg)	-7.37 ± 8.21*	-124.24 ± 81.95*	-47.82 ± 39.67	-40.30 ± 51.36*
ASP (Right leg)	1.34 ± 4.26	68.82 ± 63.46*	89.96 ± 64.69*	24.64 ± 51.59
ASP (Left leg)	-3.07 ± 9.26	-145.30 ± 110.34*	-42.02 ± 50.70*	-53.21 ± 76.38*

Fig. 1 - From top left to bottom right: musculoskeletal models during running, the side-cut manoeuvre, backwards running, vertical jumping (counter-movement and past toe-off), and acceleration from a standing position (initiation of the movement and near toe-off).

Fig. 2 - Location of the contact points under the foot of the musculoskeletal model (top left), side-view of the contact points, illustrating the offset distances (bottom left), and the point activation after established ground contact (right).

Fig. 3 (a) - Results for running, backwards running, and side-cut, illustrating the antero-posterior GRF, medio-lateral GRF, and vertical GRF. **(b)** - Results for vertical jump and acceleration from a standing position (ASP), illustrating the antero-posterior GRF, medio-lateral GRF, and vertical GRF. The predicted variables are illustrated in blue and the measured variables in red. The results are presented as the mean ± 1 SD (shaded area).

Fig. 4 (a) - Results for running, backwards running, and side-cut, illustrating the frontal GRM, sagittal GRM, and transverse GRM. **(b)** - Results for vertical jump and acceleration from a standing position (ASP), illustrating the frontal GRM, sagittal GRM, and transverse GRM. The predicted variables are illustrated in blue and the measured variables in red. The results are presented as the mean ± 1 SD (shaded area).

Fig. 5 (a) - Results for running, backwards running, and side-cut, illustrating the ankle flexion moment (AFM), subtalar eversion moment (ASEM), and knee flexion moment (KFM). **(b)** - Results for vertical jump and acceleration from a standing position (ASP), illustrating the ankle flexion moment (AFM), subtalar eversion moment (ASEM), and knee flexion moment (KFM). The variables associated with the predicted and measured GRF&Ms are illustrated in blue and red, respectively. The results are presented as the mean ± 1 SD (shaded area).

**Fig. 6 (a)** - Results for running, backwards running, and side-cut, illustrating the hip flexion moment (HFM), hip abduction moment (HAM), and hip external rotation moment (HERM). **(b)** - Results for vertical jump and acceleration from a standing position (ASP), illustrating the hip flexion moment (HFM), hip abduction moment (HAM), and hip external rotation moment

(HERM). The variables associated with the predicted and measured GRF&Ms are illustrated in blue and red, respectively. The results are presented as the mean ± 1 SD (shaded area).

Fig. 7 (a) - Results for running, backwards running, and side-cut, illustrating the ankle, knee, and hip resultant JRF. **(b)** - Results for vertical jump and acceleration from standing position (ASP), illustrating the ankle, knee, and hip resultant JRFs. The variables associated with the predicted and measured GRF&Ms are illustrated in blue and red, respectively. The results are presented as the mean ± 1 SD (shaded area).

Fig. 1

Fig. 2

35 mm offset ← | → 25 mm offset
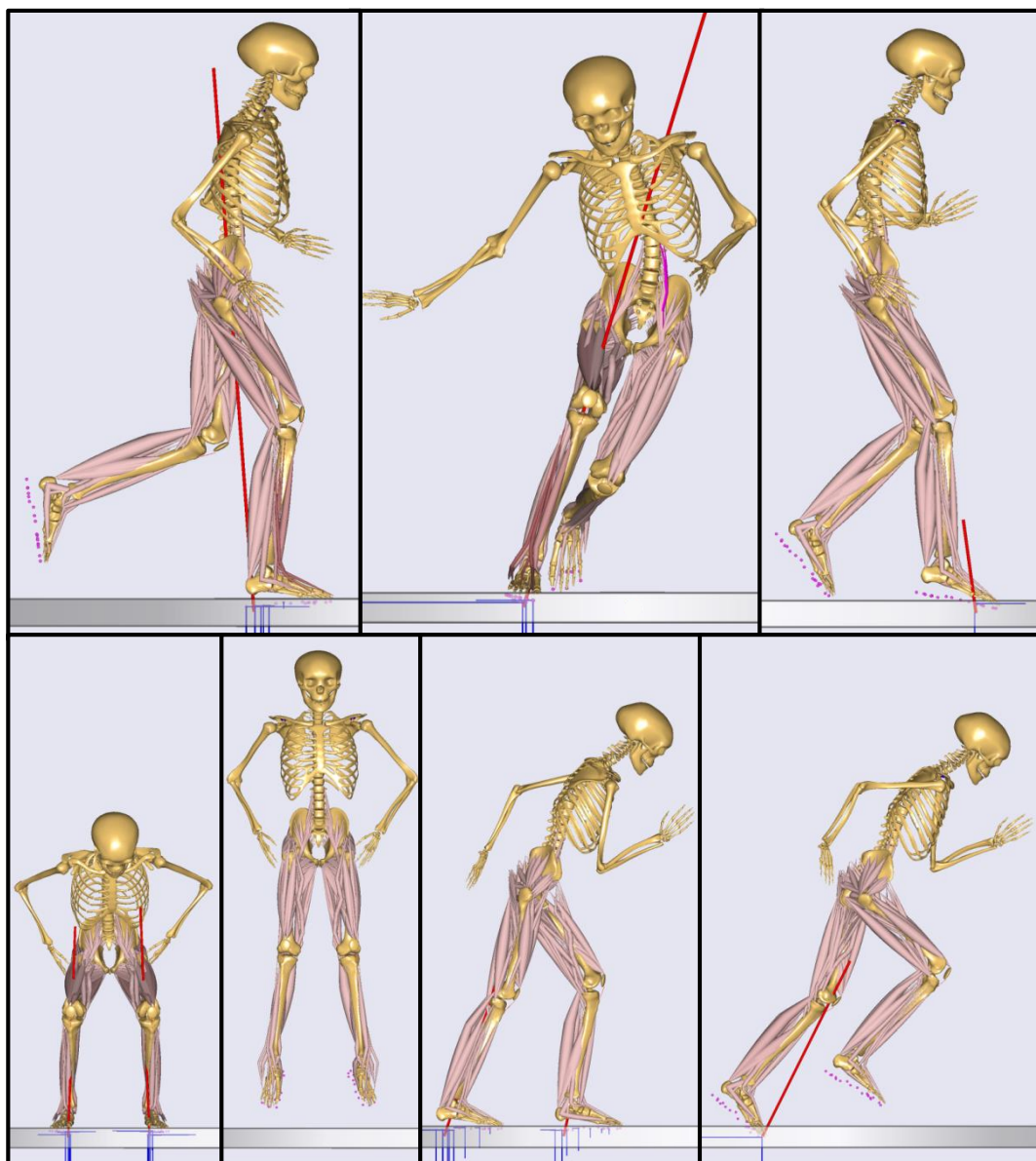
2
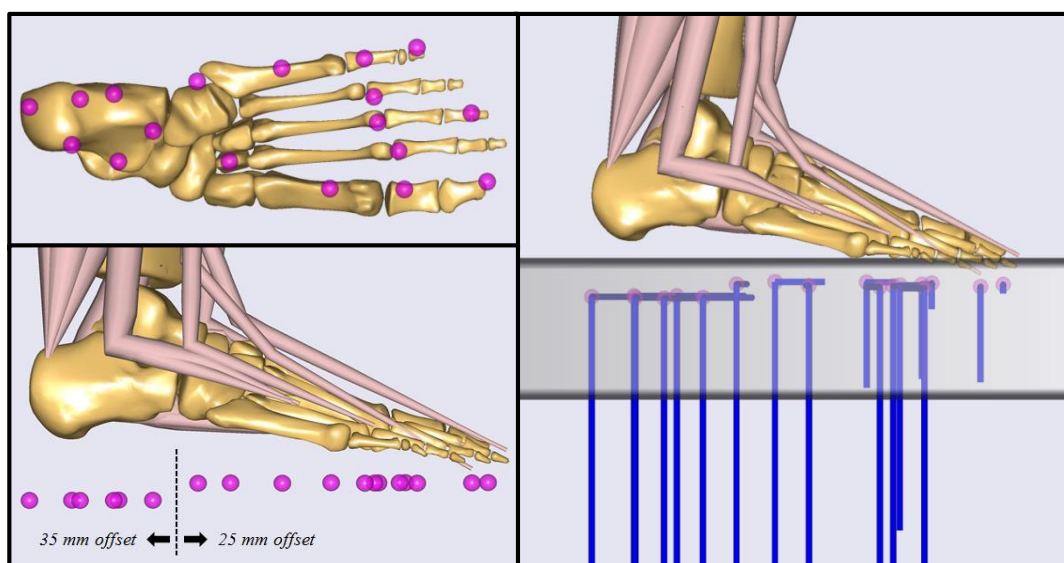
Fig. 3 (a)
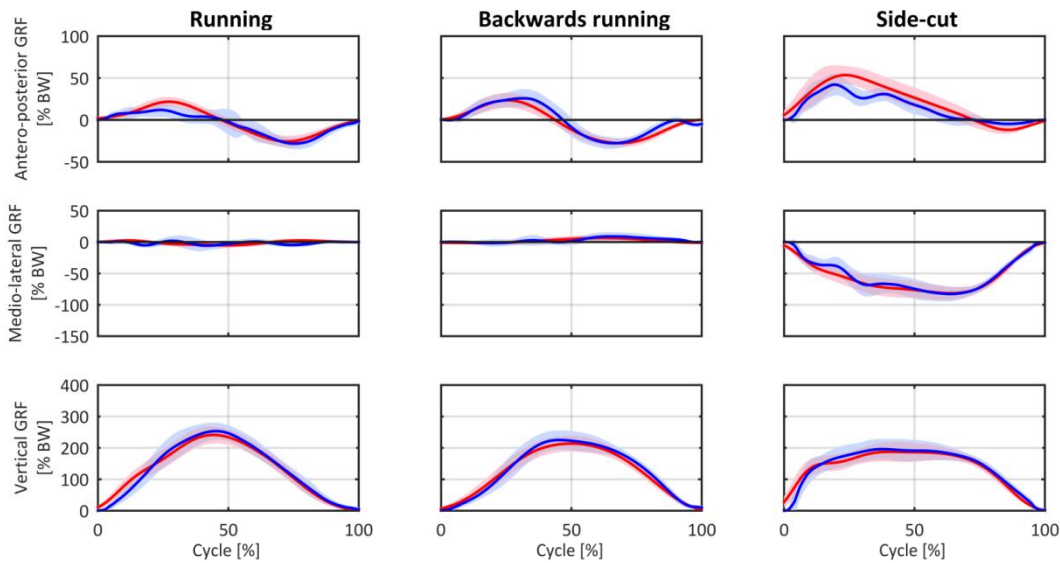
Fig. 3 (b)
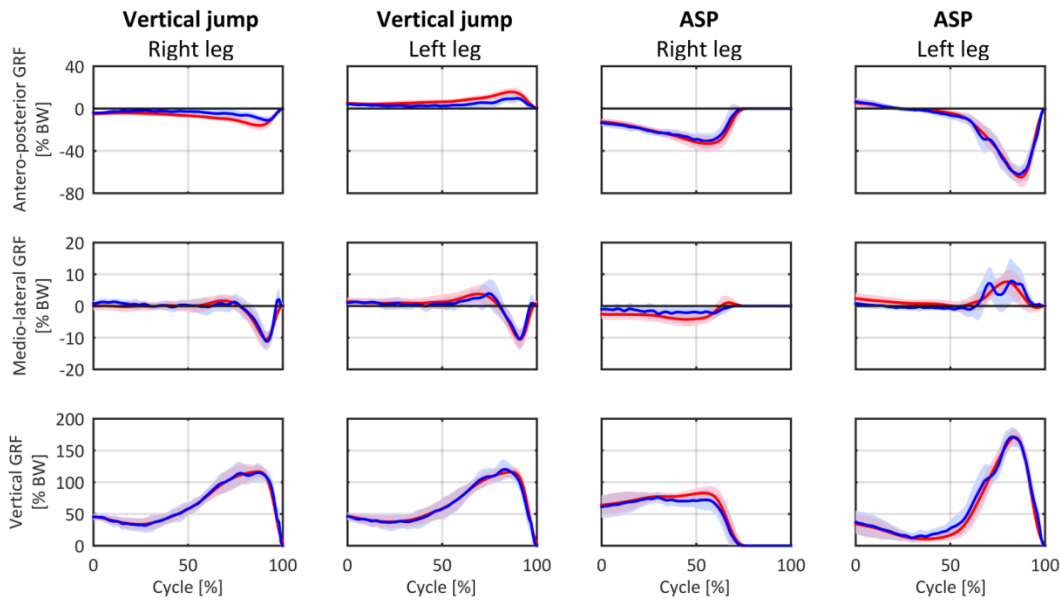
Fig. 4 (a)
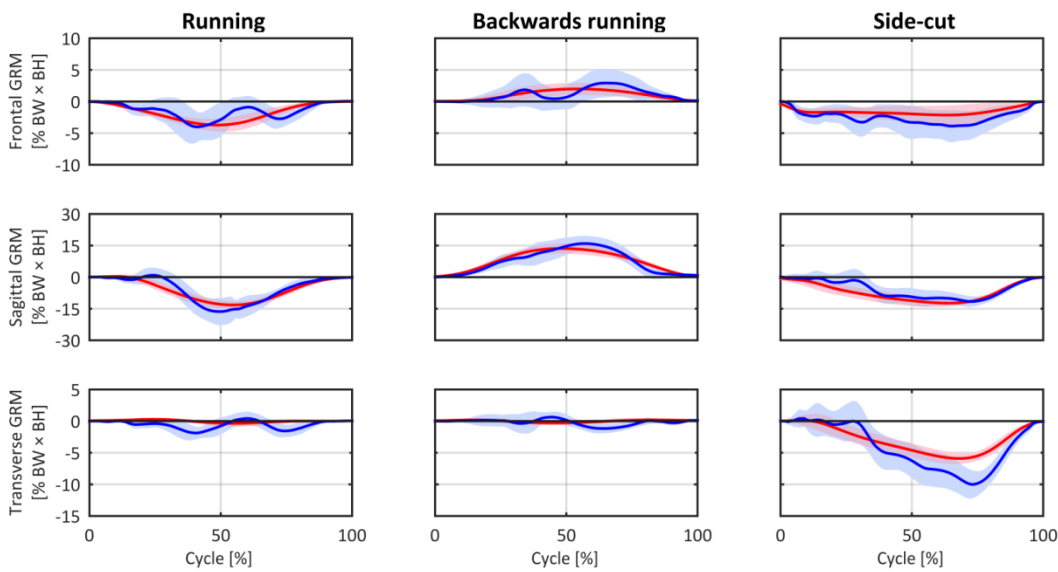
Fig. 4 (b)
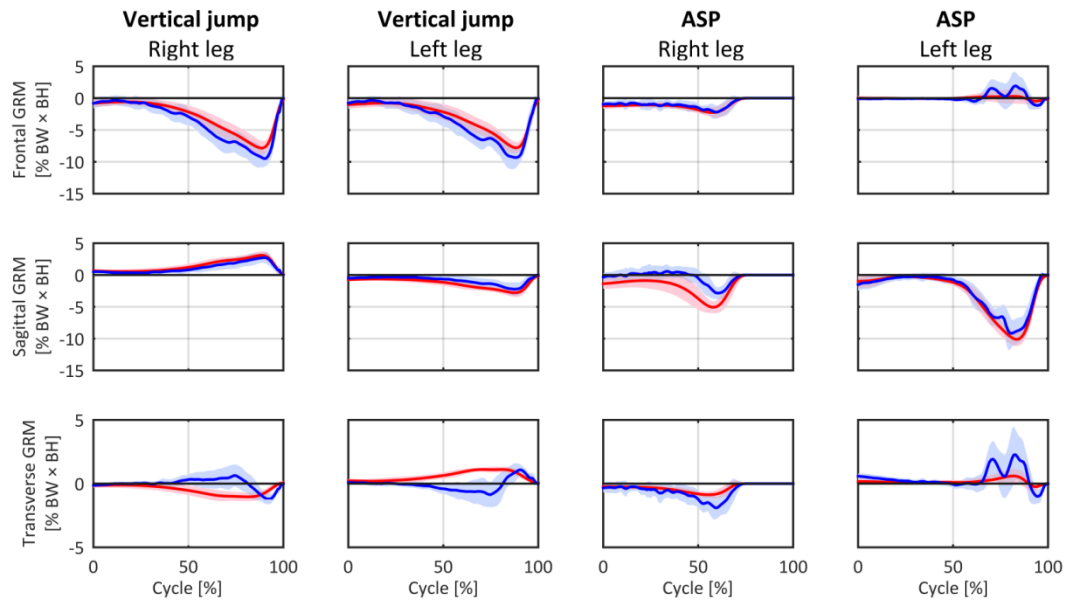
Fig. 5 (a)
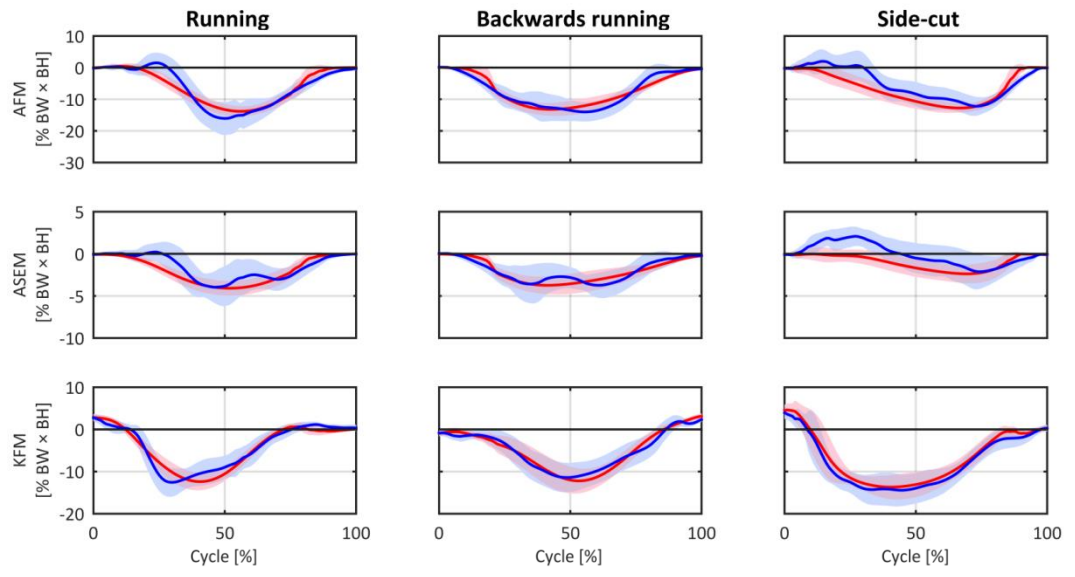
Fig. 5 (b)
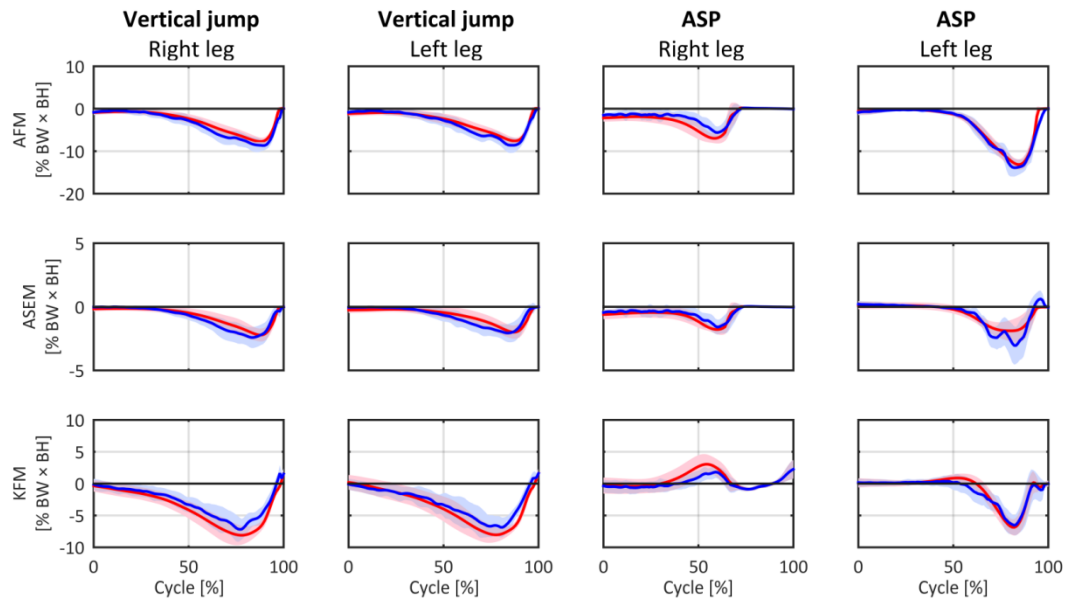
Fig. 6 (a)
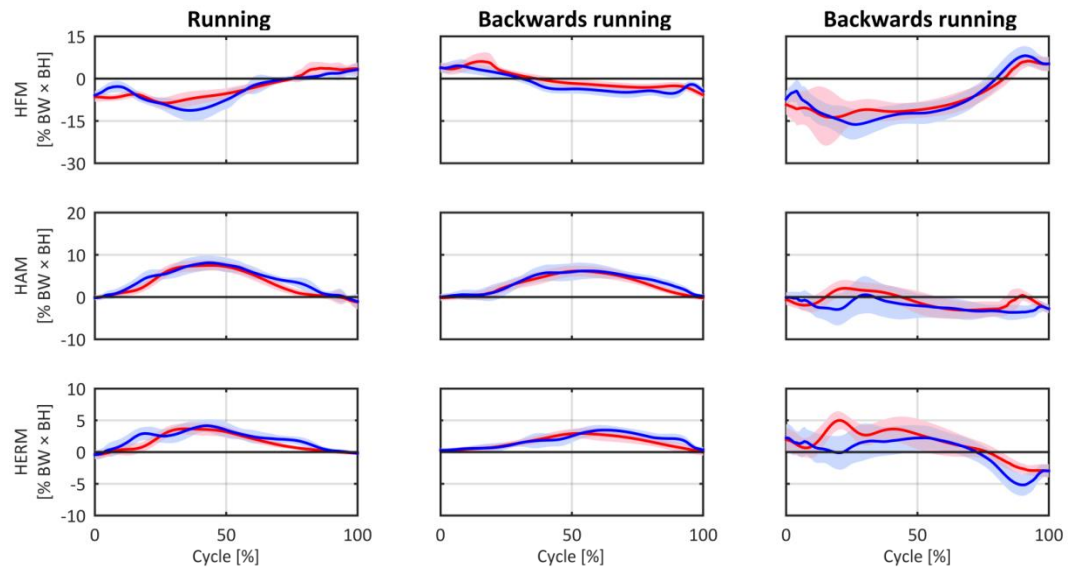
Fig. 6 (b)
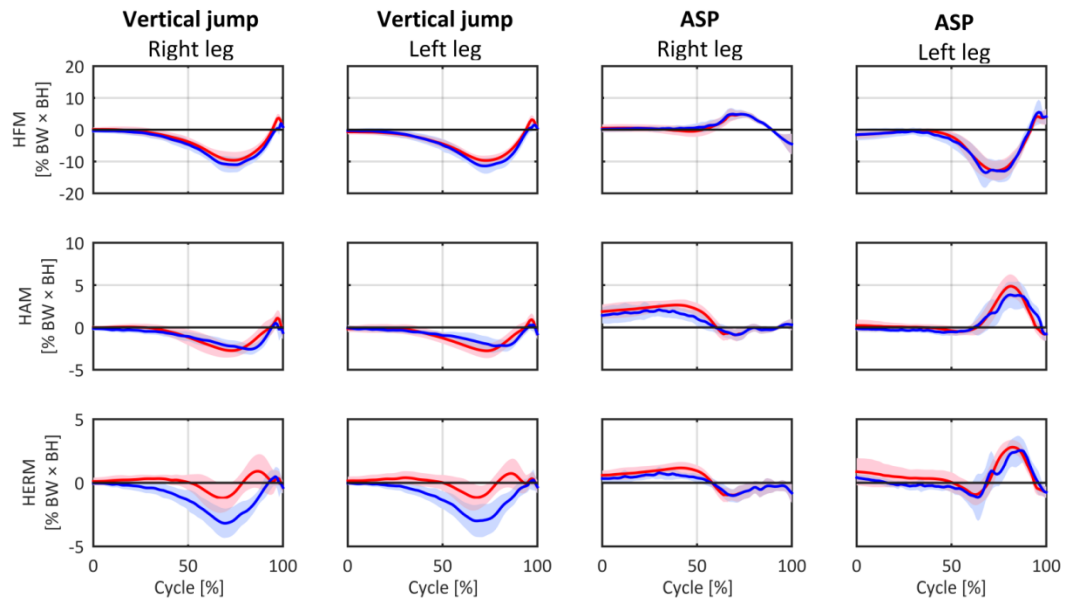
Fig. 7 (a)
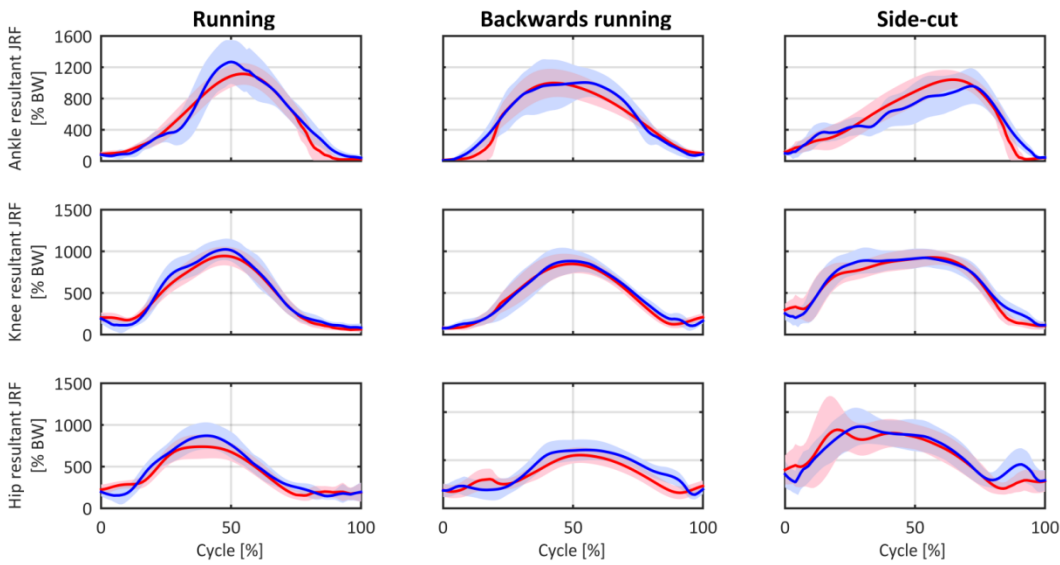
Fig. 7 (b)
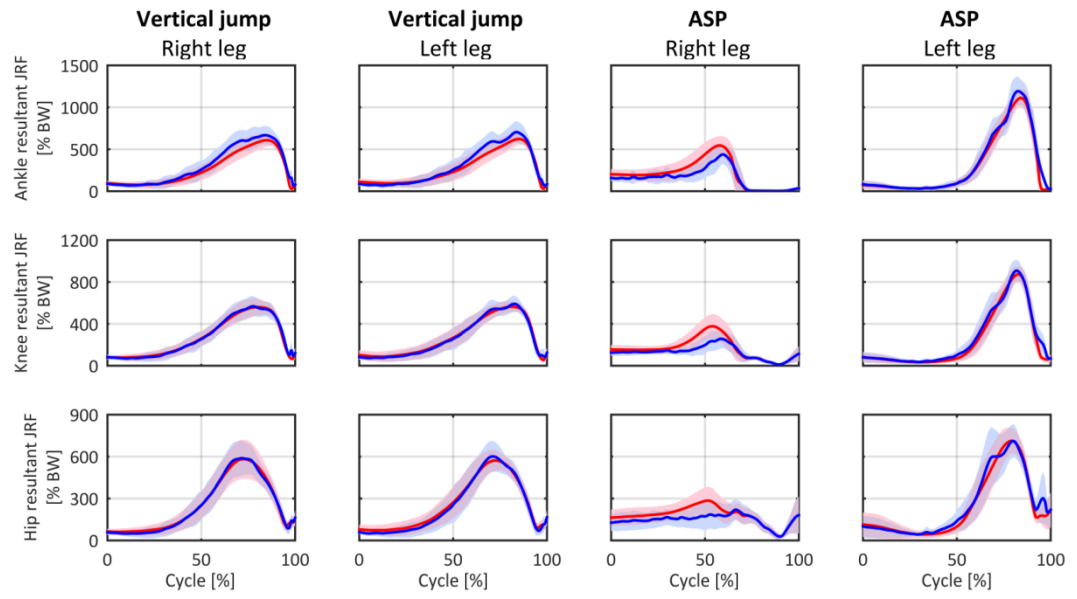
Label	Position	A-P	M-L	P-D
RTHI	Right thigh	Opt.	Opt.	Opt.
LTHI	Left thigh	Opt.	Opt.	Opt.
RKNE	Right lateral epicondyle	Fix.	Fix.	Fix.
LKNE	Left lateral epicondyle	Fix.	Fix.	Fix.
RPSI	Right posterior superior iliac spine	Fix.	Fix.	Fix.
LPSI	Left posterior superior iliac spine	Fix.	Fix.	Fix.
RASI	Right anterior superior iliac spine	Fix.	Fix.	Fix.
LASI	Left anterior superior iliac spine	Fix.	Fix.	Fix.
RANK	Right lateral malleolus	Fix.	Fix.	Fix.
LANK	Left lateral malleolus	Fix.	Fix.	Fix.
RHEE	Right calcaneus	Fix.	Fix.	Fix.
LHEE	Left calcaneus	Fix.	Fix.	Fix.
RTIB	Right tibia	Opt.	Opt.	Opt.
LTIB	Left tibia	Opt.	Opt.	Opt.
RTOE	Right metatarsus	Fix.	Fix.	Fix.
LTOE	Left metatarsus	Fix.	Fix.	Fix.
RMT5	Right fifth metatarsal	Fix.	Fix.	Fix.
LMT5	Left fifth metatarsal	Fix.	Fix.	Fix.
RELB	Right lateral epicondyle	Fix.	Fix.	Fix.
LELB	Left lateral epicondyle	Fix.	Fix.	Fix.
RWRA	Right wrist bar thumb side	Fix.	Fix.	Fix.
LWRA	Left wrist bar thumb side	Fix.	Fix.	Fix.
RFINL	Right first metacarpal	Fix.	Fix.	Fix.
LFINL	Left first metacarpal	Fix.	Fix.	Fix.
RFINM	Right fifth metacarpal	Fix.	Fix.	Fix.
LFINM	Left fifth metacarpal	Fix.	Fix.	Fix.
RUPA	Right triceps brachii	Opt.	Opt.	Opt.
LUPA	Left triceps brachii	Opt.	Opt.	Opt.
RSHO	Right Acromio-clavicular joint	Fix.	Fix.	Fix.
LSHO	Left Acromio-clavicular joint	Fix.	Fix.	Fix.
STRN	Xiphoid process of the sternum	Opt.	Opt.	Opt.
CLAV	Jugular Notch	Opt.	Opt.	Fix.
C7	7th Cervical Vertebrae	Fix.	Fix.	Fix.
RILC*	Right iliac crest	-	-	-
LILC*	Left iliac crest	-	-	-

*Excluded
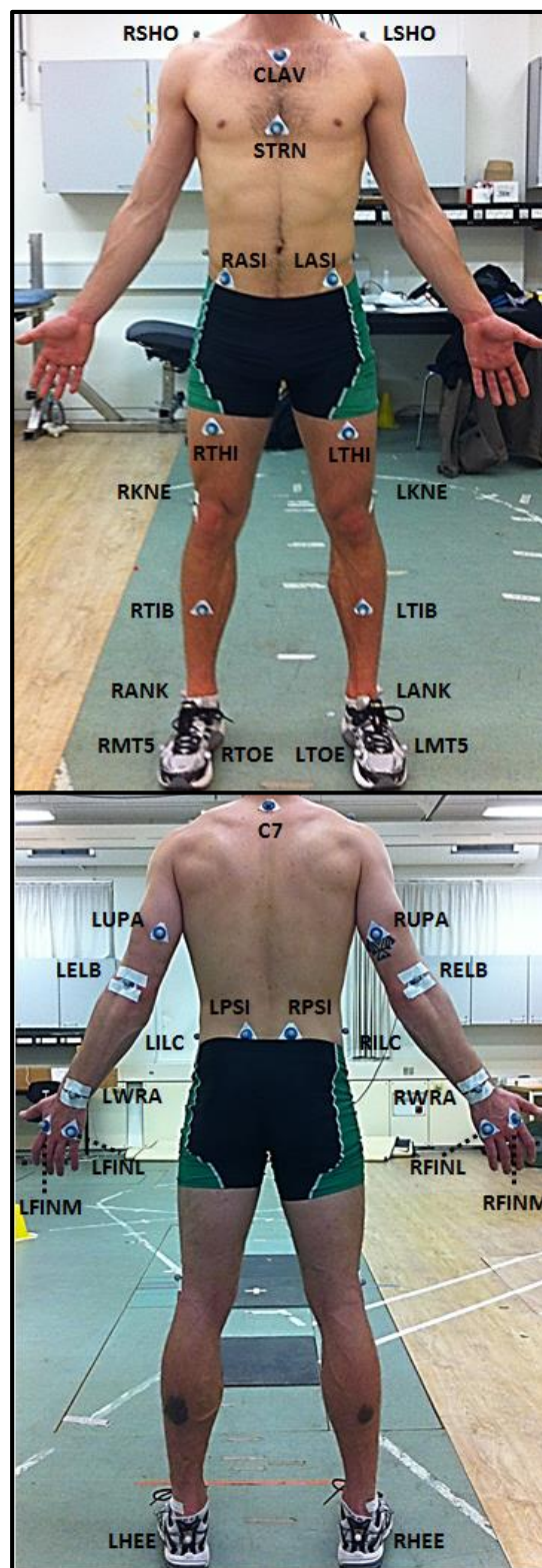
Sup. Figure 1 – Marker protocol, listing marker labels, positions, and whether the marker positions were fixed (Fix.) or optimized (Opt.) in the antero-posterior (A-P), medio-lateral (M-L), and proximal-distal (P-D) directions.